Published in final edited form as:
Wiley Interdiscip Rev Nanomed Nanobiotechnol. 2012 July ; 4(4): 448–457. doi:10.1002/wnan.1170.

Nanoformulations for molecular MRI

Chuqiao Tu[*] and **Angelique Y. Louie**
Department of Biomedical Engineering, University of California, Davis, CA 95616, USA

Abstract

Nanoscale contrast agents have shown the ability to increase the detection sensitivity of MRI by several orders of magnitude, endowing this traditionally macroscopic modality with the ability to observe unique molecular signatures. Herein, we describe three types of nanoparticulate contrast agents: iron oxide nanoparticles, gadolinium-based nanoparticles, and bio-essential manganese, cobalt, nickel, and copper ion-containing nanoformulations. Some of these agents have been approved for clinical use, but more are still under development for medical imaging. The advantages and disadvantages of each nanoformulation, in terms of intrinsic magnetism, ease of synthesis, and biodistribution, etc. are discussed.

INTRODUCTION

Magnetic resonance imaging (MRI) is a powerful tool used to differentiate diseased tissues from their surroundings by using magnetic fields and radiowaves to generate high-resolution anatomical images of the body. However, diseases frequently arise from biochemical changes at the molecular and cellular level, long before macroscopic, MRI-detectable anatomical changes occur. Contrast agents can greatly enhance the signal detection capability (sensitivity) of MRI, and the development of effective MRI contrast agents to improve detection of early disease is of great interest to diagnostic medicine.

The majority of MRI contrast agents currently available in clinics are small molecular gadolinium (Gd(III)) chelates. These are efficient MRI signal enhancers due to the lanthanide ion's large magnetic moment and slow electron spin relaxation time. However, Gd(III) chelates usually possess low relaxivities (r_1 = 3–5 mM^{-1} s^{-1} and r_2 = 5–6 mM^{-1} s^{-1}).(4) In addition, the clinical approved agents are extracellular, and generally have short serum half-lives, due to rapid renal clearance, which can result in insufficient accumulation at the region of interest (ROI).(4) The other widely used clinical agents have been polymer coated iron oxide nanoparticles.(2) The particles generate strong local magnetic field gradients which give rise to accelerated loss of phase coherence of the surrounding water proton spins, resulting in a large ionic r_2 relaxivity.(5) The surfaces of nanomaterials are readily modified and functionalized to provide biocompatibility, biostability, and specific biomarker targeting. Furthermore, the nanometer sizes can escape renal clearance mechanisms and result in a prolonged blood circulation half-life(6), greatly increasing their opportunity to arrive and accumulate at the ROI.

Recently, the concept of coupling small molecular agents to nanoparticulate scaffolds has emerged as a promising mechanism to improve contrast agent properties. In comparison with small molecular Gd(III) chelates, particulate agents tend to possess much higher relaxivities because a large amount of signal-enhancing materials can be packed into a relatively small volume. In addition, the attachment of small molecular Gd(III) agents to nanoparticles can increase ionic relaxivities as well, due to their extended rotational

[*]Correspondence to chqtu@ucdavis.edu.

correlation time τ_R. Free Gd(III) chelates have a rapid tumbling rate in solution, thus a short τ_R (~ 0.1 ns) which results in a low r_1 relaxivity. When Gd(III) chelates are encapsulated in micelles and silica or conjugated to dendrimers to form paramagnetic nanoparticulate agents, the motion of Gd(III) chelates is restricted which slows down τ_R, resulting in substantial increases in ionic (per Gd) relaxivities.(7–10) In this brief review, recent progress on new nanoformulations for molecular MRI applications will be highlighted.

IRON-BASED NANOPARTICULATE MRI CONTRAST AGENTS

Iron oxide nanoparticulate contrast agents (IO NPs) typically have a central iron oxide core that is surrounded by a carbohydrate or polymer coating that prevents aggregation of the iron oxide cores, affords water solubility, and improves biocompatibility. IO NPs are called superparamagnetic iron oxide nanoparticles (SPIO) because compared to a single paramagnetic ion, each vectorized particle bears a huge magnetic moment. SPIO are usually divided into two categories for the use as molecular MR imaging agents: standard (SSPIO, > 50 nm) and ultrasmall (USPIO, < 50 nm) SPIO.(2) SSPIO have high r_2/r_1 ratios (> 5) and are often used for passive T_2- and T_2*-weighted MR imaging (2) of liver and spleen because their large sizes cause them to be quickly taken up by reticuloendothelial system (RES) after administration. USPIO present low r_2/r_1 ratios (1–2) and their sizes allow them to avoid both renal excretion (clears particles < 8 nm) and RES clearance (clears particles > 80 nm); therefore, they have a relatively extended blood circulation time, with more time to accumulate at specific organs and tissues.(12)

SPIO are often made by reduction and co-precipitation of ferrous and ferric salts in an alkaline medium in the presence of stabilizers such as hydrophilic polymers. However, SPIO made from co-precipitation methods are fairly polydisperse, i.e. multiple iron oxide cores encapsulated within a polymer stabilization shell. More recently developed monocrystalline iron oxide nanoparticles (MION) are a subset of USPIO that have single crystal cores and hydrodynamic sizes of approximately 10–30 nm.(11) Recent advances in iron oxide particles have included new applications in disease models, and surface modifications to improve targeting to biomarkers and cells.

Dextran-coated MIONs have been studied as macrophage-targeted MRI contrast agents because they can be sequestered by macrophages *via* phagocytosis.(13) This makes these nanoparticles promising in detection of inflamed atherosclerotic plaques. Morishige et al. prepared MION-47 which has an approximate 5-nm iron oxide core coated with an approximate 10-nm thick dextran layer for MRI of a rabbit injury model.(15) The MIONs have an r_1 relaxivity of 16.5 mM^{-1} s^{-1} and an r_2 relaxivity of 34.8 mM^{-1} s^{-1} in aqueous solution at 37 °C and 0.47 T.(16) MION-47 was infused *via* an ear vein in cholesterol-fed New Zealand White rabbits 6 months after balloon injury surgery, which would induce inflamed plaques. In comparison with MRI images before administration of MION-47, *in vivo* T_2-weighted spin-echo 3T MRI visualized decreased T_2 signal intensity at abdominal aortas 72 h post-injection, whereas T_1-weighted spin-echo images showed no significant signal intensity change. The results were confirmed by histological studies that co-localized iron accumulation with immunoreactive macrophages in atheroma. What is more interesting is that treatment with Rosuvastatin for 3 months yielded diminished macrophage content and reversed T_2 signal intensity changes.(15) The results demonstrated that untargeted MIONs can be used to track inflammation in atherosclerotic plaques. Plaque inflammation can correlate with vulnerability to rupture. A high density of macrophage on atherosclerotic plaque shoulders is considered as an indicator of unstable plaques.(14)

Although SPIO have been found to accumulate in plaques *via* phagocytosis by macrophages, the uptake of these agents is non-specific; thus, the labeling efficiency for plaques is not ideal. Active targeting of nanoparticulate agents can be achieved by decorating them with ligands such as antibodies, peptides, and small molecules, etc. that have both affinity and specificity for known biomarkers associated with lesions, thus enabling them to be taken up by cells *via* more efficient receptor-mediated process. We have developed agents targeted to macrophages through scavenger receptors. The massive uptake of modified LDLs, which play an important role in the pathogenesis of atherosclerosis, by macrophages is believed to be mediated through scavenger receptor class A (SR-A), a type of protein over-expressed on the surface of activated macrophages.(17) SR-A has broad ligand specificity for a diverse array of polyanionic macromolecules, such as maleylated bovine serum albumin (mal-BSA), oxidized LDL, dextran sulfate, and polyinosinic acid, etc.(17)

We have developed a number of methods to generate dextran-sulfate coated iron oxide particles to target SR-A.(18–20) Recently, we have improved the synthesis by sulfating dextran coated iron oxide nanoparticles (DIO) with sulfur trioxide.(21) The sulfated DIO (SDIO) had an average core size of 7–8 nm, a hydrodynamic diameter of 62 nm, an r_1 relaxivity of 18.1 mM^{-1} s^{-1}, and an r_2 relaxivity of 95.8 mM^{-1} s^{-1} (37 °C, 1.4 T). Cell studies confirmed that SDIO were nontoxic and specifically taken up by macrophages *via* a receptor-mediated process, while the uptake of DIO by macrophages was limited. *In vivo* MRI of an atherosclerotic mouse injury model showed substantial signal loss on the injured carotid at 4 and 24 h post intravenous injection of SDIO (Figure 1). No discernable signal decrease was seen at the control carotid and only mild signal loss was observed for the injured carotid post-injection of non-sulfated DIO, indicating preferential uptake of the SDIO particles at the site of atherosclerotic plaque.(21) This work demonstrated the improved efficiency of SR-A targeted iron oxide nanoparticles for labeling macrophage-laden plaques in comparison with non-targeted analogues.

Besides detection and diagnosis of diseases, MRI is of interest to monitor stem cell therapies which have been heralded as potentially promising for many debilitating diseases. One of the most important challenges for regenerative medicine is to understand the fate of stem cells after transplantation. MRI could be a valuable tool for this purpose because of its advantages including non-invasive imaging, high spatial resolution, widespread availability in most clinics, and use of non-ionizing radiation. In order to visualize and track transplanted stem cells by MRI, the cells need to be labeled with a highly sensitive contrast agent prior to transplantation. Because tracking stem cells usually requires the imaging of transplanted cells *in vivo* over a relatively long time period (up to months) to monitor the cells' survival, migration, differentiation, and regenerative impact, SPIO has been widely investigated for cell labeling due to SPIO's low cytotoxicity, negligible interference with normal cellular physiology, and high sensitivity.(22, 23)

Anderson et al. labeled Sca1+ bone marrow cells with clinically approved SSPIO (ferumoxides).(24) In order to improve nanoparticle internalization, ferumoxides were modified with poly-L-lysine (PLL) through electrostatic interactions because the polycationic particles are more easily transferred into the cells by endocytosis and pinocytosis. After systemic administration of labeled cells into glioma-bearing mice, serial MRI was performed to determine the temporal-spatial distribution of administrated cells during tumor growth. Mice that had received labeled cells demonstrated hypointense regions within the tumor that evolved over time. Histology results showed that iron-labeled cells located around the tumor rim of the mice expressed endothelial markers CD31 and von Willebrand factor, indicating the transplanted cells had differentiated into endothelial-like cells.(24)

Cell-based therapy is highly valuable for the central nervous system because of the physiological importance and limited self-regeneration abilities of this system. Neri et al.

labeled human neural precursor cells (NPCs) with USPIOs (Sinerem, 20–40 nm) and SSPIO (Endorem, 80–150 nm). Efficient labeling (> 80%) and MR detection of NPCs without impairment of cell survival, proliferation, sphere-forming ability, and multipotency were achieved by lower doses of 25 and 400 μg Fe/mL and shorter incubation times of 24 and 48 h for Endorem and Sinerem, respectively, than reported similar examples. *In vivo* MRI indicated that low numbers (5×10^3 to 1×10^4) of viable SPIO-labeled NPCs could be efficiently detected after transplantation in the adult murine brain and could be tracked for at least 1 month in longitudinal studies (Figure 2).(25)

GD-BASED NANOPARTICULATE MRI CONTRAST AGENTS

Although SPIO are fairly easily synthesized and have had a safe record, they function by producing magnetic inhomogeneity due to their magnetic susceptibility, resulting in a loss of phase coherence and reduced hypointense (darker) contrast. This negative contrast mechanism precludes their use in body regions with low signals or high intrinsic magnetic susceptibility. It might also be difficult to ascribe signal loss due to SPIO with certainty in other body regions because there can be sources of signal loss in MR images other than SPIO accumulation.(26) In contrast, paramagnetic contrast agents induce hyperintense (brighter) contrast by affecting tissue relaxation through dipole-dipole interactions, molecular motion, and magnetic susceptibility. “Positive” contrast agents, such as Gd agents, are generally preferred by clinicians, because it is easier to identify signal enhancement than signal loss.(4, 27) Various Gd-based nanoparticles, such as Gd oxide nanoparticles, and Gd(III) chelates attached to dendrimers, or encapsulated in micelle or silica, have been synthesized and are used for pre-clinical MRI research.(7–9, 28–30) In comparison with small molecular Gd chelates, these nanoscale Gd agents exhibit increased relaxivity, carry higher Gd payloads, have longer circulation times, and offer selective targeting of biological sites, the properties similar to SPIO.

Dendrimers, particularly polyamidoamine (PAMAM), are a common platform for the fabrication of nanoparticulate Gd agents. They are spherical polymers consisted of highly repeated branches. Dendrimers contain known numbers of surface functional groups which allow for controlled reaction and conjugation with imaging agents.(31) The number of surface functional groups and the size of the dendrimers are determined by the generation (of branching) and can be controlled very precisely. For example, PAMAM grows from 2.2–13.5 nm through generations 1–10 (G1–G10) with the corresponding number of surface amino groups increasing from 8 to 4096.(32) The attachment of Gd(III) chelates to the surface of dendrimers has been shown to substantially increase water proton relaxation rates as well as increase serum half-life.(33, 34) For example, Nwe et al. synthesized a series of G4, G5, and G6 PAMAM dendrimers conjugated with the Gd(III)–DOTA (DOTA: 1,4,7,10-tetraazacyclododecane-1,4,7,10-tetraacetic acid).(35) The chelate to dendrimer ratios were found to be 28:1, 61:1, and 115:1 for G4, G5, and G6 PAMAM-Gd(III)-DOTA, respectively. The longitudinal ionic r_1 relaxivity measured at physiological pH were 29.6, 49.8, and 89.1 $mM^{-1}\ s^{-1}$ (22 °C, 3 T), 7–21 times higher than that of Magnevist ($r_1 \sim 4$ $mM^{-1}\ s^{-1}$), a commercial Gd contrast agent.(36) The small hydrodynamic sizes of 5.2, 6.5, and 7.8 nm for G4, 5, and 6 conjugates allow the nanoparticulate agents to be excreted by the kidney, and their blood half-lives in mice were measured to be 17.5, 38.5, and 67.7 minutes, respectively.(37)

Dendrimers with core materials other than PAMAM have also been used as scaffolds. Luo et al. reported the synthesis of peptide-constructed dendrimer-Gd(III)-DTPA that possessed highly controlled and precise structures. The agents had no obvious cytotoxicity and showed a 9-fold increase in ionic r_1 relaxivity comparing to Gd-DTPA. *In vivo* studies showed that the agent provided 54.8% enhanced signal intensity in mouse kidney 60-min post-injection. (38)

In addition to paramagnetic Gd chelated to the surface of nanoparticles as described above, Gd ions/chelates have been encapsulated in fullerenes and carbon nanotubes to form superparamagnetic Gd nanoparticles, known as gadofullerenes and gadonanotubes, respectively.(39) The common gadofullerene is Gd@C_{60} where a single Gd atom was doped in a nanoscale carbon sphere consisting of 60 carbon atoms arranged in hexagons and pentagons with an internal diameter of 0.7 nm. Due to the highly hydrophobic cavity, the mechanism for enhancement of the proton relaxation time *via* bonding of water molecules directly to the Gd^{3+} ion is impossible in gadofullerenes. Instead, the Gd atom donates three electrons to the electronegative carbon cage to become Gd^{3+} ion, making the fullerene surface paramagnetic.(40) The surface of Gd@C_{60} can be modified with hydroxyl and carboxylic acid groups, yielding Gd@$C_{60}(OH)_n$ and Gd@$C_{60}[C(COOH)_2]_{10}$, etc. to make Gd@C_{60} water-soluble. The paramagnetic carbon cage causes simultaneous relaxation of many water molecules on its surface, benefiting from its large surface area-to-volume ratio. This results in an efficacious outer-sphere relaxation process, and a significantly increased relaxivity value compared to current clinical Gd chelates.(39) Gadofullerenes were observed to form aggregates as the pH of the solution decreased from 9, resulting in increases in relaxivity because aggregation slows down the rotational correlation time τ_R. The increase in relaxivity continues until reaching a pH of 3, below which water-soluble gadofullerenes precipitate.

A few gadofullerenes have been tested *in vivo*.(41–43) Gd_3N@C_{80} is the tri-gadolinium nitride encapsulated metallo-C_{80}-fullerene which had ionic r_1 relaxivities of 34, 48, and 11 mM^{-1} s^{-1} at 0.35, 2.4 and 9.4 T, respectively.(44) Recently, carboxyl and hydroxyl groups functionalized Gd_3N@C_{80} was radiolabeled with lutetium 177 (^{177}Lu) and the resultant multimodal nanoformulation ^{177}Lu-Gd_3N@C_{80} was used for imaging-guided brachytherapy of orthotopic xenograft mouse brain tumors. The functionalized Gd_3N@C_{80} exhibited gadofullerenes' pH-dependent, dynamic aggregation and/or disaggregation behavior, as shown in Figure 3. Unlike chemotherapeutic agents that must enter cells to be active, brachytherapy only requires radionuclides to remain within an "effective range" of tumor cells for a period of time. *In vivo* MR imaging showed that 25.6% ± 1.2 of the infused ^{177}Lu-Gd_3N@C_{80} remained in the tumor 52 days post-injection, allowing for longitudinal imaging and effective brachytherapy, which was verified by extended survival time (> 2.5 times that of the untreated control group) and histological signs of radiation-induced tumor damage.(43)

Gd^{3+} ions can be loaded within the hollow interior of ultra-short single-walled carbon nanotubes (USSWNTs, 20–100 nm) but exist as superparamagnetic clusters (ca. 1–5 nm, 3–10 Gd^{3+} ions per cluster) because of the sidewall defects that are a consequence of the chemical cutting process when preparing USSWNTs. The aggregation and superparamagnetization endow gadonanotubes extremely high ionic r_1 relaxivity values, ca. 2–8 times larger than gadofullerenes or 40-times larger than Gd-DTPA.(45) Similar to gadofullerenes, the relaxivities of gadonanotubes are also highly pH-dependent; relaxivity nearly doubles from 65 mM^{-1} s^{-1} at pH 7.4 to 105 mM^{-1} s^{-1} at pH 7.0, and nearly triples at pH 6.7 at 1.5 T and 37 °C. This characteristic has been utilized for the preparation of "smart" gadonanotubes in detection of small metastasized cancerous lesions because the extracellular pH of cancerous tissue can be as low as 6.3.(46)

Recently, gadonanotubes have been applied for intracellular labeling of pig bone marrow-derived mesenchymal stem cells (MSCs).(47) *In vitro* studies showed that MSCs could be incubated with micromolar concentrations of gadonanotubes and the number of Gd^{3+} ions per cell could reach 10^9 without compromising cell viability, differentiation potential, proliferation pattern, or phenotype. The uptake of gadonanotubes by MSCs is a function of particle concentration and incubation time. Complete labeling was achieved by 4 h and the average number of Gd^{3+} ions per cell remained constant for up to 24 h of incubation. Transmission electron microscopy (TEM) visually confirmed the cellular uptake of the gadonanotubes, which appear as irregular electron-dense aggregates within the cytoplasm, as shown in Figure 4. The T_1 relaxation time of gadonanotube-labeled MSCs was found to be nearly half that of unlabeled MSCs at 1.5 T, suggesting that gadonanotubes might be suitable for *in vivo* tracking of stem cells, as well as other mammalian cell types.(48)

The carbon sheath of gadonanotubes has been functionalized for water solubility, biocompatibility, and active biomarker targeting. For example, the cyclic RGD peptide has been covalently attached to the sidewalls of gadonanotubes, making the agent potentially suitable for early detection of metastatic cancer cells.(49) In spite of interesting results and attractive perspectives, investigations of using gadonanotubes as well as gadofullerenes are still in their infancy. New methods are needed to overcome the current difficulties in synthesis and purification of these agents and to address important issues such as stability, biocompatibility, and *in vivo* safety, etc. in the near future.

BIOLOGICAL METAL-BASED NANOPARTICULATE MRI CONTRAST AGENTS

Continuing concerns on the potential toxicity of Gd contrast agents, particularly in renally compromised patients, has aroused the interest in alternatives to Gd(III) agents, with an emphasis on endogenous metals found in biology such as Mn^{2+}, Co^{2+}, Ni^{2+}, Cu^{2+}, and Zn^{2+} ion etc. which are natural cellular constituents, often acting as regulatory cofactors for enzymes and receptors. Advances in synthetic techniques that allow precise control over morphology and composition have made it possible to dope these metal ions into iron oxides, generating various nanoparticulate ferrites with a different chemical composition of the magnetic core such as manganese ferrite ($MnFe_2O_4$), cobalt ferrite ($CoFe_2O_4$), and nickel ferrite ($NiFe_2O_4$) etc. Magnetite, Fe_2O_3•FeO, crystallizes within an inverse spinel structure. The larger oxygen anions are closely packed to form a face-centered cubic unit cell and the smaller iron cations fill in the gaps, resulting in two arrangements: a tetrahedral site in which an iron cation is surrounded by 4 oxygen anions and an octahedral site in which an iron cation is surrounded by 6 oxygen anions. The tetrahedral sites are exclusively occupied by Fe^{3+} cations, while octahedral sites are alternately taken by Fe^{2+} and Fe^{3+} cations.(5) Ferrites with divalent metallic dopants such as Co^{2+} and Ni^{2+} ions will keep the same spinel structure as Fe_2O_3•FeO, while Fe_2O_3•MnO has a mixed spinel structure: tetrahedral sites are occupied by $Mn^{2+}{}_{(1-x)}Fe^{3+}{}_x$ $(0 < x < 1)$ and octahedral sites are occupied by $Mn^{2+}{}_xFe^{3+}{}_{(2-x)}$.(50) Doped ferrites usually have high magnetization and large r_2 relaxivity values. Fe_2O_3•MnO showed the strongest magnetization with an r_2 relaxivity value of 358 mM^{-1} s^{-1}. The r_2 values decreased to 218, 172, 152 and 62 mM^{-1} s^{-1}, respectively, for the samples of Fe_2O_3•FeO, Fe_2O_3•CoO, Fe_2O_3•NiO and CLIO.(50)

Nanoformulations based on these biological metal ions ($M^{2+} = Mn^{2+}$, Co^{2+}, Ni^{2+}, and Cu^{2+} ion etc.) have also been reported for MR imaging.(51–53) Similar to Gd nanoformulations, aggregation of large amount of M^{2+} ions or their derivatives in a nanoparticle can significantly increase the ionic relaxivity and the overall detection sensitivity. For example, Mn^{2+} ions doped silicon nanoparticles, Mn^{2+} ions encapsulated liposomes, “hard” Mn(II) nanoparticles, and self-assembled “soft” paramagnetic Mn(II) monomers have been reported for molecular MR imaging experiments.(54, 55)

We have doped Mn^{2+} ions in silicon quantum dots (QDs) and the resultant magnetic QDs (Si_{Mn} QDs) were coated with dextran sulfate to target them to SR-A of macrophages.(55, 56) The Si_{Mn} QDs have a hydrodynamic diameters ranging from 8.3 to 43 nm, an ionic r_1 relaxivity of 25.50 mM^{-1} s^{-1}, and an ionic r_2 relaxivity of 89.01 mM^{-1} s^{-1} (37 °C, 1.4 T). Cell studies showed that Si_{Mn} QDs were taken up by macrophages via a receptor-mediated process, and produced distinct contrast in both T_1-weighted MR and single- or two-photon excitation fluorescence images.(55) Pan et al. prepared paramagnetic nanocolloids consisting of Mn(II) oxide (ManOC) or Mn(II) oleate (ManOL) coated with phospholipids. Hydrodynamic sizes for ManOC and ManOL are 136 and 134 nm, respectively. The ionic r_1 relaxivities of ManOC and ManOL at 3 T and 25 °C were 4.1 and 14.6 mM^{-1} s^{-1}, and the particulate relaxivities were approximate 91,127 and 423,420 mM^{-1} s^{-1}, respectively. The good sensitivity displayed by the two nanoformulations, particularly the ManOL particles whose sensitivity could extend to 3.7 nM, was demonstrated *via* the *in vitro* visualization of human thrombi by T_1-weighted MRI using biotinylated ManOC and ManOL, as shown in Figure 5.(51)

CONCLUDING REMARKS

In this review, we have illustrated the ability of nanoscale contrast agents to improve detection sensitivity and MRI image contrast. Several nanoformulations for molecular MR imaging have been highlighted. Each system has its own advantages and disadvantages in terms of intrinsic magnetism, ease of synthesis, toxicity, and biodistribution, etc. To date, superparamagnetic iron oxide nanoparticles are the only nanoscale contrast agents approved for clinical MRI because they are composed of biodegradable iron, which is biocompatible and can thus be reused/recycled by cells using normal biochemical pathways for iron metabolism (Table 1).(2)

Although there has been renewed interest in bio-essential Mn^{2+}, Co^{2+}, Ni^{2+}, and Cu^{2+} ion-based nanoparticulate MRI agents, the inferior inherent magnetism of these biological metal ions compared to Gd^{3+} and the difficulty in finding ligands able to bind these ions with strength higher than those shown by naturally occurring endogenous substrates limits enthusiasm for their adoption. Today Gd-based small molecule chelates remain the most popular MRI contrast agents in clinics in spite of their low sensitivity. The development of Gd-based nanoparticulate agents has been somewhat tepid because an apparent problem is that the corresponding large sizes accompanied with increased Gd-loading will result in a prolonged circulation half-life of Gd^{3+} ions or Gd(III) chelates in the body. This is good for targeted MRI, but may cause safety concerns because extended retention of Gd(III) agents in the body. Therefore, the pharmacokinetic behavior and biostability should be the paramount considerations when pursuing new assemblies that contain maximum Gd(III)-loading.

While exploring the design of novel nanoparticulate MRI agents, new roads should be paved toward the development of alternatives for molecular MRI. For example, one promising method is the combined PET and MRI system that has shown great advantages in comparison with single imaging modality alone, because the combined system possesses both detection sensitivity and spatial resolution.(57) PET nucleotide labeled magnetic nanoparticles have been prepared and applied for PET guided MR imaging of atherosclerotic plaques, tumors, etc.(58) The highly sensitive PET enables rapid visualization of the probes' *in vivo* distribution, which allows one to guide the high-resolution MR imaging to a small volume of interest, greatly reducing the MRI scan time and dosage requirement for contrast agents.

Acknowledgments

The authors wish to acknowledge the NIH-NIBIB (R01 EB000993) for support of this work.

References

1. Chan KWY, Wong WT. Small molecular gadolinium(III) complexes as MRI contrast agents for diagnostic imaging. Coord Chem Rev. 2007; 251(17–20):2428–51.
2. Burtea, C.; Laurent, S.; Elst, LV.; Muller, RN. Contrast Agents: Magnetic Resonance. In: Semmler, W.; Schwaiger, M., editors. Molecular Imaging I: Handbook of Experimental Pharmacology. Heidelberg: Springer-Verlag Berlin; 2008. p. 135-65.
3. Tu CQ, Osborne EA, Louie AY. Activatable T (1) and T (2) Magnetic Resonance Imaging Contrast Agents. Ann Biomed Eng. 2011; 39(4):1335–48. [PubMed: 21331662]
4. Caravan P, Ellison JJ, McMurry TJ, Lauffer RB. Gadolinium(III) chelates as MRI contrast agents: Structure, dynamics, and applications. Chem Rev. 1999; 99(9):2293–352. [PubMed: 11749483]
5. Gossuin Y, Gillis P, Hocq A, Vuong QL, Roch A. Magnetic resonance relaxation properties of superparamagnetic particles. Wiley Interdiscip Rev-Nanomed Nanobiotechnol. 2009; 1(3):299–310. [PubMed: 20049798]
6. Tu, C.; Louie, AY. Nanobiomaterials for Dual-mode Molecular Imaging: Advances in Probes for MR/Optical Imaging Applications. In: Sitharaman, B., editor. Nanobiomaterials Handbook. Boca Raton: CRC Press/Taylor & Francis Group; 2011. p. 1-29.
7. Bui T, Stevenson J, Hoekman J, Zhang SR, Maravilla K, Ho RJY. Novel Gd Nanoparticles Enhance Vascular Contrast for High-Resolution Magnetic Resonance Imaging. PLoS One. 2010; 5(9):e13082. [PubMed: 20927340]
8. Villaraza AJL, Bumb A, Brechbiel MW. Macromolecules, Dendrimers, and Nanomaterials in Magnetic Resonance Imaging: The Interplay between Size, Function, and Pharmacokinetics. Chem Rev. 2010; 110(5):2921–59. [PubMed: 20067234]
9. Na HB, Hyeon T. Nanostructured T1 MRI contrast agents. Journal of Materials Chemistry. 2009; 19(35):6267–73.
10. Bumb A, Brechbiel MW, Choyke P. Macromolecular and dendrimer-based magnetic resonance contrast agents. Acta Radiol. 2010; 51(7):751–67. [PubMed: 20590365]
11. Thorek DLJ, Chen A, Czupryna J, Tsourkas A. Superparamagnetic iron oxide nanoparticle probes for molecular imaging. Ann Biomed Eng. 2006; 34(1):23–38. [PubMed: 16496086]
12. Longmire M, Choyke PL, Kobayashi H. Clearance properties of nano-sized particles and molecules as imaging agents: considerations and caveats. Nanomedicine. 2008; 3(5):703–17. [PubMed: 18817471]
13. Chen W, Cormode DP, Fayad ZA, Mulder WJM. Nanoparticles as magnetic resonance imaging contrast agents for vascular and cardiac diseases. Wiley Interdiscip Rev-Nanomed Nanobiotechnol. 2011; 3(2):146–61.
14. Libby P, Okamoto Y, Rocha VZ, Folco E. Inflammation in Atherosclerosis: Transition From Theory to Practice. Circ J. 2010; 74(2):213–20. [PubMed: 20065609]
15. Morishige K, Kacher DF, Libby P, Josephson L, Ganz P, Weissleder R, et al. High-Resolution Magnetic Resonance Imaging Enhanced With Superparamagnetic Nanoparticles Measures Macrophage Burden in Atherosclerosis. Circulation. 2010; 122(17):1707–15. [PubMed: 20937980]
16. Shen T, Weissleder R, Papisov M, Bogdanov A, Brady TJ. MONOCRYSTALLINE IRON-OXIDE NANOCOMPOUNDS (MION) - PHYSICOCHEMICAL PROPERTIES. Magn Reson Med. 1993; 29(5):599–604. [PubMed: 8505895]
17. de Winther MPJ, van Dijk KW, Havekes LM, Hofker MH. Macrophage scavenger receptor class A - A multifunctional receptor in atherosclerosis. Arterioscler Thromb Vasc Biol. 2000; 20(2):290–7. [PubMed: 10669623]
18. Jarrett BR, Correa C, Ma KL, Louie AY. In Vivo Mapping of Vascular Inflammation Using Multimodal Imaging. PLoS One. 2010; 5(10):Article Number: e13254.

19. Jarrett BR, Frendo M, Vogan J, Louie AY. Size-controlled synthesis of dextran sulfate coated iron oxide nanoparticles for magnetic resonance imaging. Nanotechnology. 2007; 18(3):Article Number: 035603.
20. Jarrett BR, Gustafsson B, Kukis DL, Louie AY. Synthesis of Cu-64-labeled magnetic nanoparticles for multimodal imaging. Bioconjugate Chem. 2008; 19(7):1496–504.
21. Tu C, Ng TSC, Sohi HK, Palko HA, House A, Jacobs RE, et al. Receptor-targeted Iron Oxide Nanoparticles for Molecular MR Imaging of Inflamed Atherosclerotic Plaques. Biomaterials. 2011; 32(29):7209–16. [PubMed: 21742374]
22. Berman SMC, Walczak P, Bulte JWM. Tracking stem cells using magnetic nanoparticles. Wiley Interdiscip Rev-Nanomed Nanobiotechnol. 2011; 3(4):343–55. [PubMed: 21472999]
23. Mahmoudi M, Hosseinkhani H, Hosseinkhani M, Boutry S, Simchi A, Journeay WS, et al. Magnetic Resonance Imaging Tracking of Stem Cells in Vivo Using Iron Oxide Nanoparticles as a Tool for the Advancement of Clinical Regenerative Medicine. Chem Rev. 2011; 111(2):253–80. [PubMed: 21077606]
24. Anderson SA, Glod J, Arbab AS, Noel M, Ashari P, Fine HA, et al. Noninvasive MR imaging of magnetically labeled stem cells to directly identify neovasculature in a glioma model. Blood. 2005; 105(1):420–5. [PubMed: 15331444]
25. Neri M, Maderna C, Cavazzin C, Deidda-Vigoriti V, Politi LS, Scotti G, et al. Efficient in vitro labeling of human neural precursor cells with superparamagnetic iron oxide particles: Relevance for in vivo cell tracking. Stem Cells. 2008; 26(2):505–16. [PubMed: 17975226]
26. Cormode DP, Skajaa T, Fayad ZA, Mulder WJM. Nanotechnology in Medical Imaging Probe Design and Applications. Arterioscler Thromb Vasc Biol. 2009; 29(7):992–1000. [PubMed: 19057023]
27. Hermann P, Kotek J, Kubicek V, Lukes I. Gadolinium(III) complexes as MRI contrast agents: ligand design and properties of the complexes. Dalton Transactions. 2008; (23):3027–47. [PubMed: 18521444]
28. Sharma P, Brown SC, Walter G, Santra S, Scott E, Ichikawa H, et al. Gd nanoparticulates: from magnetic resonance imaging to neutron capture therapy. Adanced Powder Technology. 2007:663–98.
29. Mody VV, Nounou MI, Bikram M. Novel nanomedicine-based MRI contrast agents for gynecological malignancies. Adv Drug Deliv Rev. 2009; 61(10):795–807. [PubMed: 19427886]
30. Shao YZ, Liu LZ, Song SQ, Cao RH, Liu H, Cui CY, et al. A novel one-step synthesis of Gd(3+)-incorporated mesoporous SiO(2) nanoparticles for use as an efficient MRI contrast agent. Contrast Media Mol Imaging. 2011; 6(2):110–8. [PubMed: 21504064]
31. Barrett T, Ravizzini G, Choyke PL, Kobayashi H. Dendrimers in Medical Nanotechnology Application of Dendrimer Molecules in Bioimaging and Cancer Treatment. IEEE Eng Med Biol Mag. 2009; 28(1):12–22. [PubMed: 19150767]
32. Bosman AW, Janssen HM, Meijer EW. About dendrimers: Structure, physical properties, and applications. Chem Rev. 1999; 99(7):1665–88. [PubMed: 11849007]
33. Swanson SD, Kukowska-Latallo JF, Patri AK, Chen CY, Ge S, Cao ZY, et al. Targeted gadolinium-loaded dendrimer nanoparticles for tumor-specific magnetic resonance contrast enhancement. Int J Nanomed. 2008; 3(2):201–10.
34. Kaneshiro TL, Jeong EK, Morrell G, Parker DL, Lu ZR. Synthesis and Evaluation of Globular Gd-DOTA-Monoamide Conjugates with Precisely Controlled Nanosizes for Magnetic Resonance Angiography. Biomacromolecules. 2008; 9(10):2742–8. [PubMed: 18771313]
35. Nwe K, Bryant LH, Brechbiel MW. Poly(amidoamine) Dendrimer Based MRI Contrast Agents Exhibiting Enhanced Relaxivities Derived via Metal Preligation Techniques. Bioconjugate Chem. 2010; 21(6):1014–7.
36. Bryant LH, Brechbiel MW, Wu CC, Bulte JWM, Herynek V, Frank JA. Synthesis and relaxometry of high-generation (G = 5, 7, 9, and 10) PAMAM dendrimer-DOTA-gadolinium chelates. JMRI-J Magn Reson Imaging. 1999; 9(2):348–52.
37. Nwe K, Milenic D, Bryant LH, Regino CAS, Brechbiel MW. Preparation, characterization and in vivo assessment of Gd-albumin and Gd-dendrimer conjugates as intravascular contrast-enhancing agents for MRI. J Inorg Biochem. 2011; 105(5):722–7. [PubMed: 21463567]

38. Luo K, Liu G, She WC, Wang QY, Wang G, He B, et al. Gadolinium-labeled peptide dendrimers with controlled structures as potential magnetic resonance imaging contrast agents. Biomaterials. 2011; 32(31):7951–60. [PubMed: 21784511]
39. Matson ML, Wilson LJ. Nanotechnology and MRI contrast enhancement. Future Med Chem. 2010; 2(3):491–502. [PubMed: 21426177]
40. Bolskar RD. Gadofullerene MRI contrast agents. Nanomedicine. 2008; 3(2):201–13. [PubMed: 18373426]
41. Zhang JF, Fatouros PP, Shu CY, Reid J, Owens LS, Cai T, et al. High Relaxivity Trimetallic Nitride (Gd(3)N) Metallofullerene MRI Contrast Agents with Optimized Functionality. Bioconjugate Chem. 2010; 21(4):610–5.
42. Fatouros PP, Corwin FD, Chen ZJ, Broaddus WC, Tatum JL, Kettenmann B, et al. In vitro and in vivo imaging studies of a new endohedral metallofullerene nanoparticle. Radiology. 2006; 240(3): 756–64. [PubMed: 16837672]
43. Shultz MD, Wilson JD, Fuller CE, Zhang JY, Dorn HC, Fatouros PP. Metallofullerene-based Nanoplatform for Brain Tumor Brachytherapy and Longitudinal Imaging in a Murine Orthotopic Xenograft Model. Radiology. 2011; 261(1):136–43. [PubMed: 21813738]
44. Stevenson S, Stephen RR, Amos TM, Cadorette VR, Reid JE, Phillips JP. Synthesis and purification of a metallic nitride fullerene BisAdduct: Exploring the reactivity of Gd3N@C-80. J Am Chem Soc. 2005; 127(37):12776–7. [PubMed: 16159252]
45. Sitharaman B, Kissell KR, Hartman KB, Tran LA, Baikalov A, Rusakova I, et al. Superparamagnetic gadonanotubes are high-performance MRI contrast agents. Chem Commun. 2005; (31):3915–7.
46. Hartman KB, Laus S, Bolskar RD, Muthupillai R, Helm L, Toth E, et al. Gadonanotubes as ultrasensitive pH-smart probes for magnetic resonance imaging. Nano Lett. 2008; 8(2):415–9. [PubMed: 18215084]
47. Tran LA, Krishnamurthy R, Muthupillai R, Cabreira-Hansen MD, Willerson JT, Perin EC, et al. Gadonanotubes as magnetic nanolabels for stem cell detection. Biomaterials. 2010; 31(36):9482–91. [PubMed: 20965562]
48. Hassan AA, Chan BTY, Tran LA, Hartman KB, Ananta JS, Mackeyev Y, et al. Serine-derivatized gadonanotubes as magnetic nanoprobes for intracellular labeling. Contrast Media Mol Imaging. 2010; 5(1):34–8. [PubMed: 20101755]
49. Mackeyev Y, Hartman KB, Ananta JS, Lee AV, Wilson LJ. Catalytic Synthesis of Amino Acid and Peptide Derivatized Gadonanotubes. J Am Chem Soc. 2009; 131(24):8342. [PubMed: 19492838]
50. Lee JH, Huh YM, Jun Y, Seo J, Jang J, Song HT, et al. Artificially engineered magnetic nanoparticles for ultra-sensitive molecular imaging. Nat Med. 2007; 13(1):95–9. [PubMed: 17187073]
51. Pan DPJ, Senpan A, Caruthers SD, Williams TA, Scott MJ, Gaffney PJ, et al. Sensitive and efficient detection of thrombus with fibrin-specific manganese nanocolloids. Chem Commun. 2009; (22):3234–6.
52. Pan D, Caruthers SD, Senpan A, Yalaz C, Stacy AJ, Hu G, et al. Synthesis of NanoQ, a Copper-Based Contrast Agent for High-Resolution Magnetic Resonance Imaging Characterization of Human Thrombus. J Am Chem Soc. 2011; 133(24):9168–71. [PubMed: 21599030]
53. Wu HX, Zhang CX, Jin L, Yang H, Yang SP. Preparation and magnetic properties of cobalt nanoparticles with dendrimers as templates. Mater Chem Phys. 2010; 121(1–2):342–8.
54. Pan DPJ, Caruthers SD, Senpan A, Schmieder AH, Wickline SA, Lanza GM. Revisiting an old friend: manganese-based MRI contrast agents. Wiley Interdiscip Rev-Nanomed Nanobiotechnol. 2011; 3(2):162–73.
55. Tu CQ, Ma XC, Pantazis P, Kauzlarich SM, Louie AY. Paramagnetic, Silicon Quantum Dots for Magnetic Resonance and Two-Photon Imaging of Macrophages. J Am Chem Soc. 2010; 132(6): 2016–23. [PubMed: 20092250]
56. Tu CQ, Ma XC, House A, Kauzlarich SM, Louie AY. PET Imaging and Biodistribution of Silicon Quantum Dots in Mice. ACS Med Chem Lett. 2011; 2(4):285–8. [PubMed: 21546997]

NIH-PA Author Manuscript
NIH-PA Author Manuscript

NIH-PA Author Manuscript

NIH-PA Author Manuscript

57. Cherry SR, Louie AY, Jacobs RE. The integration of positron emission tomography with magnetic resonance imaging. Proceedings of the Ieee. 2008; 96(3):416–38.
58. Louie A. Multimodality Imaging Probes: Design and Challenges. Chem Rev. 2010; 110(5):3146–95. [PubMed: 20225900]

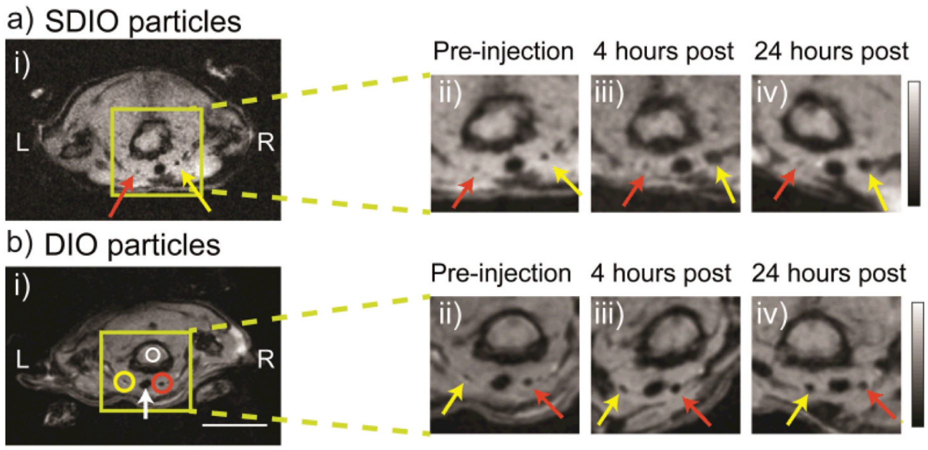

FIGURE 1.

Signal change in MRI over time after (a) SDIO or (b) DIO injection. The ligated carotid artery is denoted by the yellow arrow and the control carotid artery is denoted by the red arrow. Circles indicate the ROI measures used to derive the contrast ratio (CR) metric. (Scale bar = 10 mm. L = left, R = right, green box shows magnification area, white arrow denotes the trachea). (Reproduced with permission from Ref (21). Copyright 2011 Elsevier Ltd.)

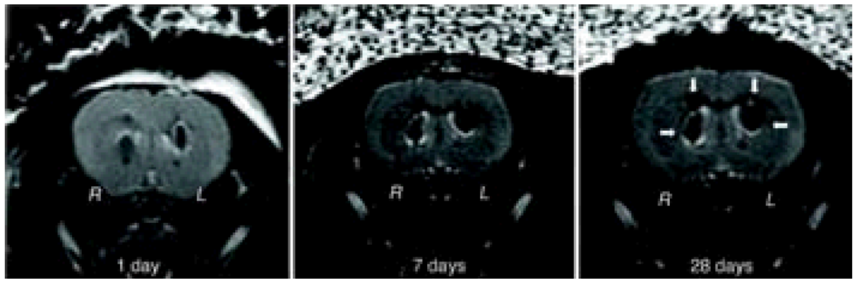

FIGURE 2.

SPIO-labeled human neural precursor stem cells can be tracked in longitudinal MR studies. Mice were stereotactically implanted in R hemisphere with 2.5×10^3 viable Endorem-labeled cells and in the contralateral hemisphere (L) with the same number of cells labeled with Endorem plus PLL. One day after implantation, cells were detectable at the injection sites as hypointense spots in T_2 images. The MR signal remained stable up to the latest time point (28 days) analyzed. (Reproduced with permission from Ref (25). Copyright 2008 John Wiley & Sons, Inc.)

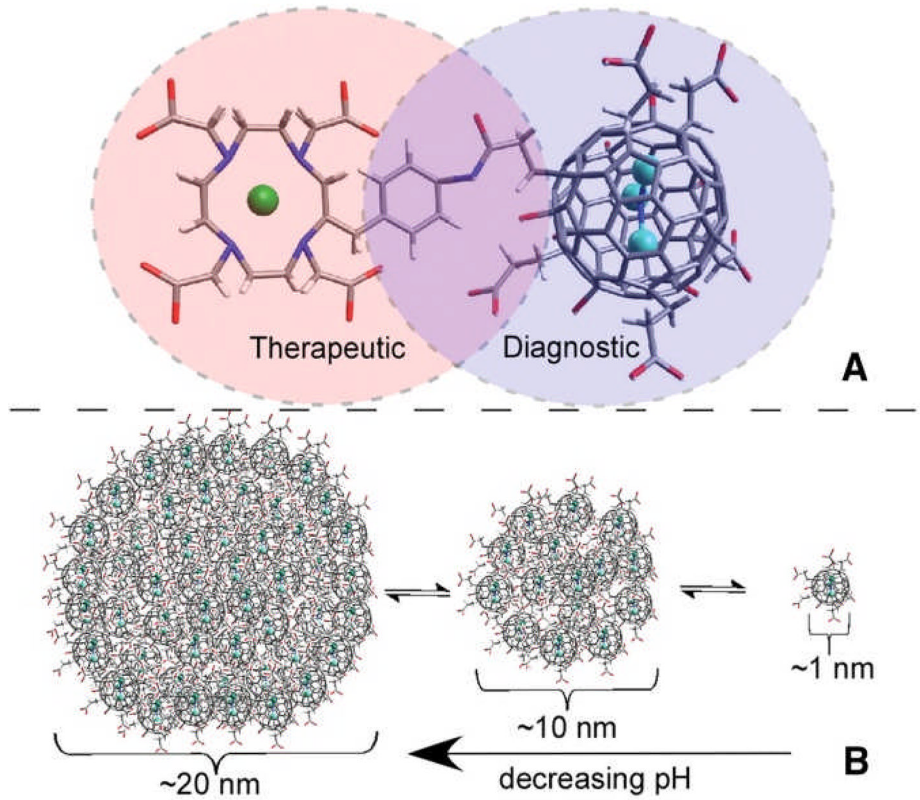

Figure 3.
(A). Structural representation of the trimetallic nitride template metallofullerene–based heranostic agent $Gd_3N@C_{80}$. Therapeutic, covalent linkage, and diagnostic regions are denoted by pink, purple, and blue, respectively. (B). Dynamic equilibrium of aqueous clustering properties of $Gd_3N@C_{80}$, which shifts to larger clusters with decreasing pH. (Reproduced with permission from Ref (43). Copyright 2011 Radiological Society of North America).

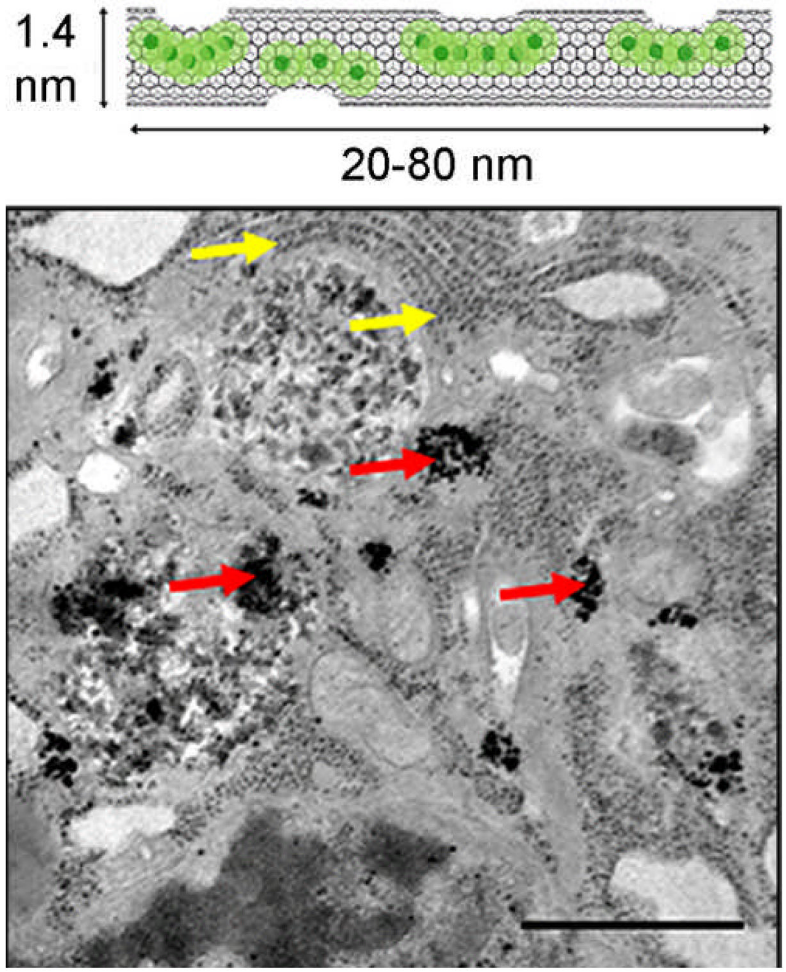

FIGURE 4.

(A). A representative illustration of gadonanotubes. Clusters of internally-loaded Gd^{3+} ions are located at defect sites along the nanocapsule sidewalls. (B). TEM images of a gadonanotube-labeled MSC. Red arrows point to gadonanotube aggregates in the cytoplasm. Yellow arrows point to ribosomes of the endoplasmic reticulum. Scale bar = 1 μm. (Reproduced with permission from Ref (47). Copyright 2011 Elsevier B.V.).

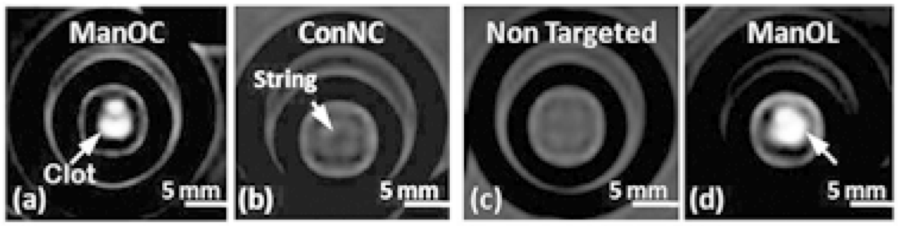

Figure 5.

T_1-weighted gradient echo MRI images of fibrin-targeted nanocolloids: (a) ManOC; (b) Control nanocolloid (ConNC, no MnO or Mn-oleate); (c) non-targeted-ManOL (no biotin) and (d) ManOL, bound to cylindrical plasma clots measured at 3 T. (Reproduced with permission from Ref (51). Copyright 2009 Royal Society of Chemistry).

TABLE 1

Properties of nanoparticulate MRI contrast agents approved for clinical use or under clinical evaluation.(2, 8)

Generic name (Short name)	Brand name	Relaxivity ($mM^{-1}s^{-1}$) (0.47 T, 37 °C)		Size (nm)	Half-life (Dosage (μmol Fe/kg))	Target	Location (Status)
		r_1	r_2				
Ferumoxide (AMI-25)	Endorem Feridex	10.1	120	80–150	2 h 30	Liver/Spleen, perfusion, angiopgraphy	US and Europe (Discontinued)
Ferumoxsil (AMI-121)	Lumirem Gastromark	N/A	N/A	300	Oral	Gastrointestinal	US and Europe
Ferumoxtran (AMI-227)	Sinerem Combidex	9.9	65	20–40	24–36 h 45	Lymph nodes, Angiopgraphy	US and Europe (Discontinued)
Ferumoxytol (AMI-228)	Feraheme	15	89	30	10–14 h 18–74	Iron replacement	US (iron therapy)
Ferrixan Ferucarbotran (SHU 555A)	Resovist Cliavist	9.7	189	60	2.4–3.6 h 8–12	Liver	Europe, Japan, and Australia
(SHU 555C)	Supravist Clariscan	10.7	38	21	6 h (40)	Angiopgraphy perfusion, angiopgrphy	Phase III complete
Feruglose (NC100150)		N/A	N/A	20	6 h (36)		Phase II complete (Discontinued)